

The effect of Se ↔ Te substitution on crystallisation micro-mechanisms evincing in GeTe₄ glass

Roman Svoboda¹ · Daniela Brandová¹ · Ludvík Beneš^{2,3} · Jiří Málek¹

Received: 16 April 2015 / Accepted: 3 August 2015 / Published online: 14 August 2015
© Akadémiai Kiadó, Budapest, Hungary 2015

Abstract Isothermal and non-isothermal crystallisation behaviour of the GeTe_{3.9}Se_{0.1} chalcogenide glass was studied dependent on particle size and compared to the similar DSC study performed for the pure GeTe₄ material. The effect of the Se ↔ Te substitution led to a decrease in the crystallisation process complexity in the case of powdered materials—the addition of Se led to domination of the slower nucleation–growth crystallisation mechanism over the fast autocatalytic growth from mechanically induced defects. The nature of the crystallisation mechanisms was confirmed by infrared microscopy and XRD. The addition of selenium into the GeTe₄ matrix caused an enlargement of the identified crystallites; this, together with the overall deceleration of the crystallisation processes, indicates the suppression of nucleation processes. The presence of Se also greatly enhanced domination of the CNT-based three-dimensional growth of volume-located crystallites. The obtained findings provide a very good explanation for the markedly increased thermal stability of Se-doped Ge–Te infrared glasses.

Keywords Crystallisation kinetics · DSC · Infrared microscopy · XRD · GeTe_{3.9}Se_{0.1} · Se–Te substitution

Introduction

Infrared optics belongs among the most important applications of chalcogenide glasses. Nowadays, telluride glasses are the focus of interest due to the fact that they provide an extension of the transmission window beyond the 16- μm borderline that is characteristic for selenides. [1] Fully telluride chalcogenide matrices are, however, rather poor glass-formers, and only a few compositions can be utilised to create stable bulk glass ingots that are suitable for, for example, fibre drawing or lens moulding. One of the most promising systems in this regard is selenium-doped GeTe₄. [2–7] Despite the great potential of the materials from the Te-rich side of the GeTe₄–GeSe₄ pseudo-binary line, very few studies dealing with the thermal properties of these glasses can be found in the literature [8–10] (only the characteristic temperatures are, however, reported in most cases).

Processing and shaping of bulk chalcogenide glasses requires a great deal of information about the thermal properties and thermomechanical characteristics of the given materials. In the current article, the influence of the initial Se ↔ Te substitution on the non-isothermal and isothermal crystallisation kinetics of the GeTe₄ glass will be studied by differential scanning calorimetry (DSC), X-ray diffraction analysis (XRD) and infrared microscopy. The influence of the Se ↔ Te substitution will be derived based on a comparison of the results obtained for the GeTe_{3.9}Se_{0.1} and GeTe₄ infrared glasses. The research will follow our previous findings [11, 12], dealing with the crystallisation kinetics of the base GeTe₄ glass.

Electronic supplementary material The online version of this article (doi:10.1007/s10973-015-4962-9) contains supplementary material, which is available to authorized users.

✉ Roman Svoboda
roman.svoboda@atlas.cz; roman.svoboda@upce.cz

¹ Department of Physical Chemistry, Faculty of Chemical Technology, University of Pardubice, Studentská 573, 532 10 Pardubice, Czech Republic

² Joint Laboratory of Solid State Chemistry, Institute of Macromolecular Chemistry, Academy of Sciences of the Czech Republic v.v.i., 532 10 Pardubice, Czech Republic

³ University of Pardubice, 532 10 Pardubice, Czech Republic

Theory

Crystallisation kinetics is usually studied by differential scanning calorimetry, DSC. The data can then be described according to the following equation [13]:

$$\Phi = \Delta H \cdot A \cdot e^{-E/RT} \cdot f(\alpha) \quad (1)$$

where Φ is the measured heat flow, ΔH is the crystallisation enthalpy, A is the pre-exponential factor, E is the apparent activation energy of the process, R is the universal gas constant, T is temperature and $f(\alpha)$ stands for an expression of a kinetic model with α being conversion.

In the first step of kinetic analysis, the apparent activation energy of crystallisation E is determined. In the present work, we will use the Kissinger [14], Friedman [15] and modified Kissinger–Akahira–Sunose (KAS) [16] methods described by the following equations, respectively. The original Kissinger method is only applicable under non-isothermal conditions and is based on the shift of the maximum of the crystallisation peak T_p with heating rate q^+ , according to the following equation:

$$\ln\left(\frac{q^+}{T_p^2}\right) = -\frac{E}{RT_p} + \text{const.} \quad (2)$$

$$\ln(\Phi_\alpha) = -\frac{E}{RT_\alpha} + \text{const.} \quad (3)$$

$$\ln\left(\frac{q^+}{T_x^{1.92}}\right) = -1.0008 \frac{E}{RT_x} + \text{const.} \quad (4)$$

where q^+ is heating rate, T_p is the temperature corresponding to the maximum of the crystallisation peak and Φ_α and T_x are the specific heat flow and temperature corresponding to a certain chosen value of conversion α .

In the second step of kinetic analysis, an appropriate kinetic model for the description of crystallisation peaks is determined. The characteristic kinetic functions $z(\alpha)$ and $y(\alpha)$ can be fittingly utilised in this regard. [17, 18] For non-isothermal and isothermal conditions, these functions are obtained by the following transformation of experimental data, respectively:

$$y(\alpha) = \Phi \cdot e^{E/RT} \quad (5a)$$

$$y(\alpha) = \Phi \quad (5b)$$

$$z(\alpha) = \Phi \cdot T^2 \quad (6a)$$

$$z(\alpha) = \Phi \cdot t \quad (6b)$$

With regard to the crystallisation behaviour previously reported for the GeTe_4 glass, the following models need to be considered in the present study: the physically meaningful nucleation–growth Johnson–Mehl–Avrami (JMA) model [19–22], the semi-empirical autocatalytic Šesták–Berggren (AC) model [13], the reaction order (RO) model

[23] and the power law (P) model [23], which can be described by the following equations, respectively.

$$f(\alpha) = m(1 - \alpha)[- \ln(1 - \alpha)]^{1-(1/m)} \quad (7)$$

$$f(\alpha) = \alpha^M(1 - \alpha)^N \quad (8)$$

$$f(\alpha) = (1 - \alpha)^n \quad (9)$$

$$f(\alpha) = \alpha^n \quad (10)$$

More details about the above-described methods of kinetic analysis can be found in [24].

Experimental

The $\text{GeTe}_{3.9}\text{Se}_{0.1}$ and GeTe_4 glasses were prepared by the melt-quenching technique (annealing at 950 °C for 24 h, quenching in cold water). The prepared glasses were ground and sieved (using a set of sieves with defined mesh sizes) so that the following powder fractions were obtained: 0–20, 20–50, 50–125, 125–180, 180–250, 250–300 and 300–500 μm . Small pieces of glass broken off the main glass ingot were used as “bulk” samples (in this way, the minimum number of mechanical defects and heterogeneities serving as nucleation/crystallisation centres was present). The bulk samples were assigned an average size $d_{\text{aver}} = 1$ mm for further comparisons. Amorphous character of the glasses was confirmed by XRD; homogeneity of the glass was verified based on the invariability of T_g (glass transition temperature) measured for several randomly chosen bulk samples.

The crystallisation behaviour was studied using a Q2000 heat-flow DSC (TA Instruments) equipped with an autosampler, RCS90 cooling accessory and T-zero technology. The instrument was calibrated using In, Zn and H_2O ; dry N_2 was used as purge gas at a flow rate of 50 $\text{cm}^3 \text{min}^{-1}$. Fresh zero-line calibration was performed before the measurements. Thin layer of the powder was spread on the bottom of the aluminium pans to improve thermal contact. The masses of the samples varied between 8 and 10 mg. During the non-isothermal DSC measurements, the sample was first equilibrated at 100 °C and then heated to 450 °C (above melting point) at various defined heating rates. The applied heating rates were as follows: 0.5, 1, 2, 3, 5, 7, 10, 15, 20 and 30 $^\circ\text{C min}^{-1}$. Acquisition of the DSC crystallisation peaks data was achieved by using the cubic spline interpolation of the DSC thermokinetic background. In the case of isothermal measurements, the sample was first subjected to a 5-min isotherm at 170 °C and then heated at 100 $^\circ\text{C min}^{-1}$ to a selected temperature, T_i , where the sample was allowed to isothermally crystallise until the process was complete. The isothermal crystallisation temperature range was

210–280 °C with a 10 °C step covering the range for the GeTe_{3.9}Se_{0.1} glass and 205–245 °C with a 5 °C step covering this range for the GeTe₄ glass. Very good reproducibility of the experimental data was achieved.

X-ray diffraction (XRD) analysis of amorphous and crystalline samples was performed using a Bruker AXS diffractometer D8 Advance equipped with a horizontal goniometer and scintillation counter utilising CuK_α radiation. In order to examine the development of the crystallisation process, an infrared microscope Olympus BX51 equipped with XM10 camera was used in the reflection mode.

Results and discussion

Thermal characterisation

In the first section, the overall thermal behaviour of the two studied compositions will be briefly described. Examples of raw non-isothermal DSC curves measured for the two compositions at 10 °C min⁻¹ are shown in Fig. 1. The upper two overlapping curves in Fig. 1a correspond to the measurements obtained for the 125- to 180-μm powder (dashed line) and bulk sample (solid line) of the GeTe₄ glass; the lower two overlapping lines then correspond to the GeTe_{3.9}Se_{0.1} composition. The other three graphs in Fig. 1 then display zoomed temperature intervals corresponding to the three particular thermokinetic processes of interest—glass transition, cold crystallisation and melting. Starting the comparison with the glass transition region (Fig. 1b), it is apparent that the glass transition temperature is not affected by the initial Se ↔ Te substitution. This indicates the large similarity of the base glassy structures. This is easily understandable, since both selenium and tellurium exhibit analogous coordination with preferred bonding arrangements, while forming similar structural units. The crystallisation peaks (see Fig. 1c), on the other hand, shift to significantly higher temperatures with the addition of selenium. It is also apparent that the shape of the peaks changes markedly for both of the displayed particle size fractions. The nature of the origin of this change can be partially explained by the shape of the corresponding melting peaks (Fig. 1d). Whereas the crystallisation peaks provide information about the kinetics, or the pathway to the crystalline state, the melting peaks correspond to the thermodynamic part of the process, i.e. the actual quality of the final crystallites. The increased number of melting peaks occurring in case of the GeTe_{3.9}Se_{0.1} composition indicates several distinct crystalline phases being formed during the crystallisation process. Identification of the particular phases will be discussed later in “[Identification of the crystallisation processes](#)” section.

The data depicted in Fig. 1 can also be used to calculate glass stability (GS) of the studied materials. In the present work, the three most important GS criteria will be used in this regard: Hrubý [25], Weinberg [26] and Lu and Liu [27]. In a recent study, we tested these criteria with respect to the influence of the particle size; we concluded that it is the Hrubý criterion which is least affected by the shift of the characteristic temperatures caused due to the change of the particle size. In addition, it was also confirmed that the bulk samples best represent the overall materials behaviour. The values of the three criteria calculated for the two present compositions are listed in Table 1 together with the values obtained based on the recently introduced GFA criterion [28, 29]. It is clear from the data that the addition of selenium to the GeTe₄ matrix leads to the large increase in the glass stability and glass-forming ability (GFA); while the Se ↔ Te substitution lowers the melting point of the GeTe₄ matrix, it also inhibits the crystallisation process, shifting it to higher temperatures.

Kinetic analysis

In the second section, the detailed kinetic analysis of the crystallisation processes manifesting for the two studied compositions will be presented. In Fig. 2, the results regarding the determined activation energies are presented. The upper row shows the data for GeTe₄; the lower row then corresponds to the evaluations performed for the GeTe_{3.9}Se_{0.1} composition. The left-side graphs show the activation energies plotted dependent on particle size. In the case of the GeTe₄ glass (Fig. 2a), the activation energies show almost no variation with d_{aver} (except for the two finest powder fraction). Apparently, all of the applied methodologies provided similar E values, which were consistent with the results obtained for the isothermal measurements. In the case of the GeTe_{3.9}Se_{0.1} composition (Fig. 2c), on the other hand, a strong dependence of E on d_{aver} occurs. This usually indicates a change of the dominant crystallisation process leading to the formation of a significantly different crystalline phase. This assumption is further supported by the significantly deviated higher and lower values of E evaluated according to Friedman for the isothermal and non-isothermal data, respectively. Due to the Φ_x being incorporated into the left-hand term in Eq. (3), this differential isoconversional method is very sensitive to complexity caused by changes in kinetic mechanisms. [28–36] The marked difference between the E_{Friedman} results provided for isothermal and non-isothermal data indicates the presence of multiple overlapping competing processes with significantly different activation energies. In addition, the assumption of the increased crystallisation complexity is further confirmed by the actual $E - \alpha$ and $\log A - \alpha$ dependences constructed for

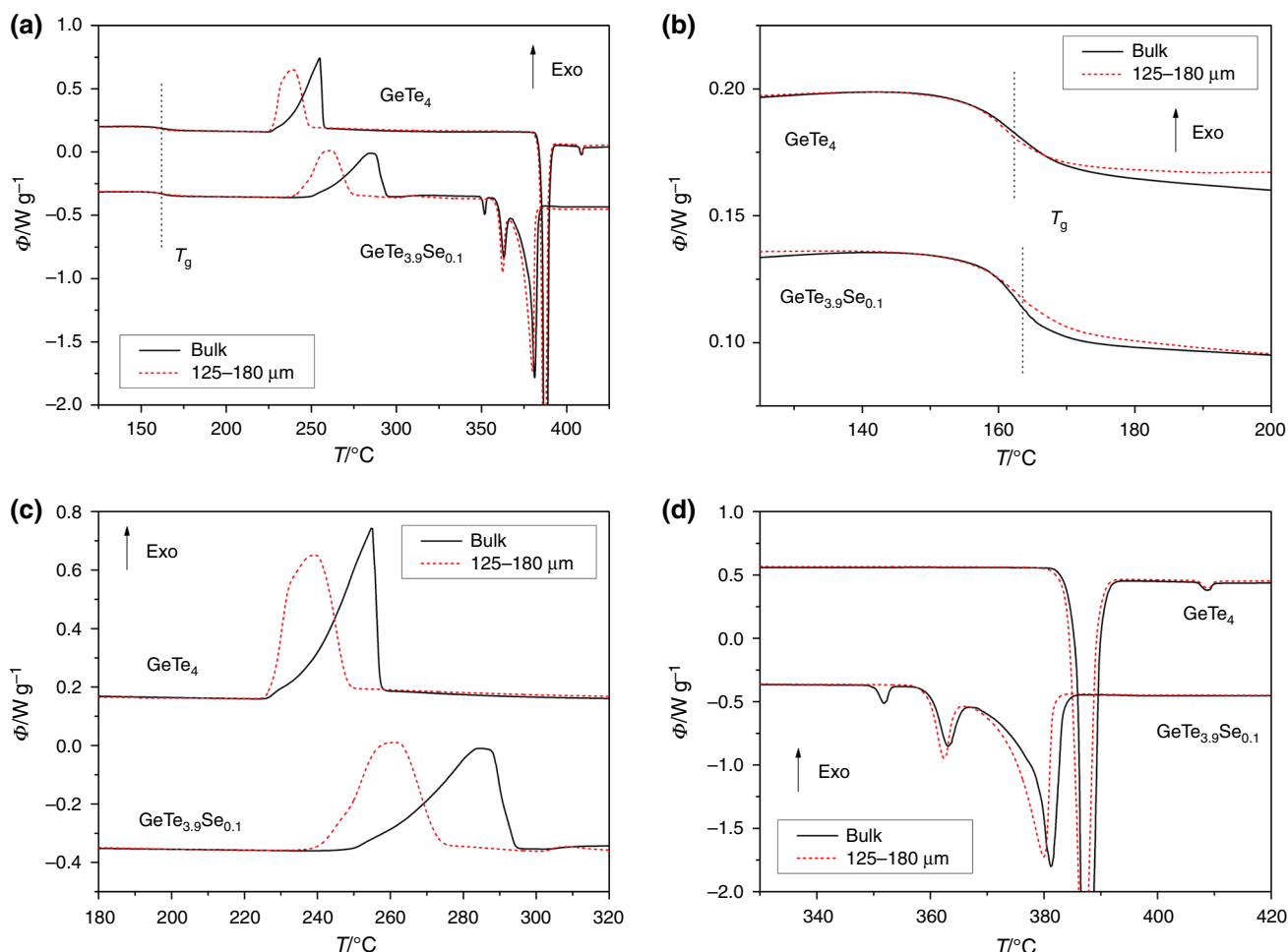


Fig. 1 Example DSC curves measured at a heating rate of 10 °C min^{-1} for the 125- to 180- μm powder and bulk sample of the two studied compositions. Exothermic effects evolve in the “upwards” direction. **a** The overall DSC curves (the glass transition

region is suggested by the *vertical dashed line*). **b–d** then display zoomed glass transition, crystallisation and melting regions, respectively

Table 1 Hrubý K_H , Weinberg K_W , Lu and Liu K_{LL} and GFA glass stability criteria calculated for the two studied glasses

	K_H	K_W	K_{LL}	GFA
$\text{Ge}_{20}\text{Te}_{80}$	0.539	0.120	0.469	0.350
$\text{Ge}_{20}\text{Te}_{78}\text{Se}_2$	0.997	0.156	0.500	0.499

The data obtained at 10 °C min^{-1} for the 125- to 180- μm powders are evaluated

each studied powder (see Supplemental online material), where in case of the $\text{GeTe}_{3.9}\text{Se}_{0.1}$ composition significant evolution of the two respective kinetic quantities with α occurs. Note that usage of the $n_{\text{JMA}} - \alpha$ dependences would be inappropriate since only model-free quantities possess interpretative possibilities with respect to the complex processes. [24] The E values obtained by means of the original Kissinger method will be used in further kinetic calculations.

In Fig. 2b, d, the so-called Kissinger plots are displayed for the GeTe_4 and $\text{GeTe}_{3.9}\text{Se}_{0.1}$ compositions, respectively (temperatures corresponding to the maxima of crystallisation peaks T_p are plotted in dependence on heating rate q^+). The same scaling of the X axis allows comparison of the temperature shifts of the crystallisation process for all particle sizes of both of the studied compositions—even the very small $\text{Se} \leftrightarrow \text{Te}$ substitution apparently inhibits the crystallisation of the GeTe_4 matrix, shifting it to significantly higher temperatures. Whereas the Kissinger plot for the GeTe_4 composition (Fig. 2b) shows a typical evolution of T_p with both q^+ and d_{aver} , the situation is completely different for the $\text{GeTe}_{3.9}\text{Se}_{0.1}$ composition (Fig. 2d). At low heating rates, a crystallisation mechanism completely independent from d_{aver} occurs; with the increase in q^+ , different crystallisation mechanisms start to dominate, exhibiting a significant $T_p - d_{\text{aver}}$ dependence. This indicates a large degree of complexity of the overall

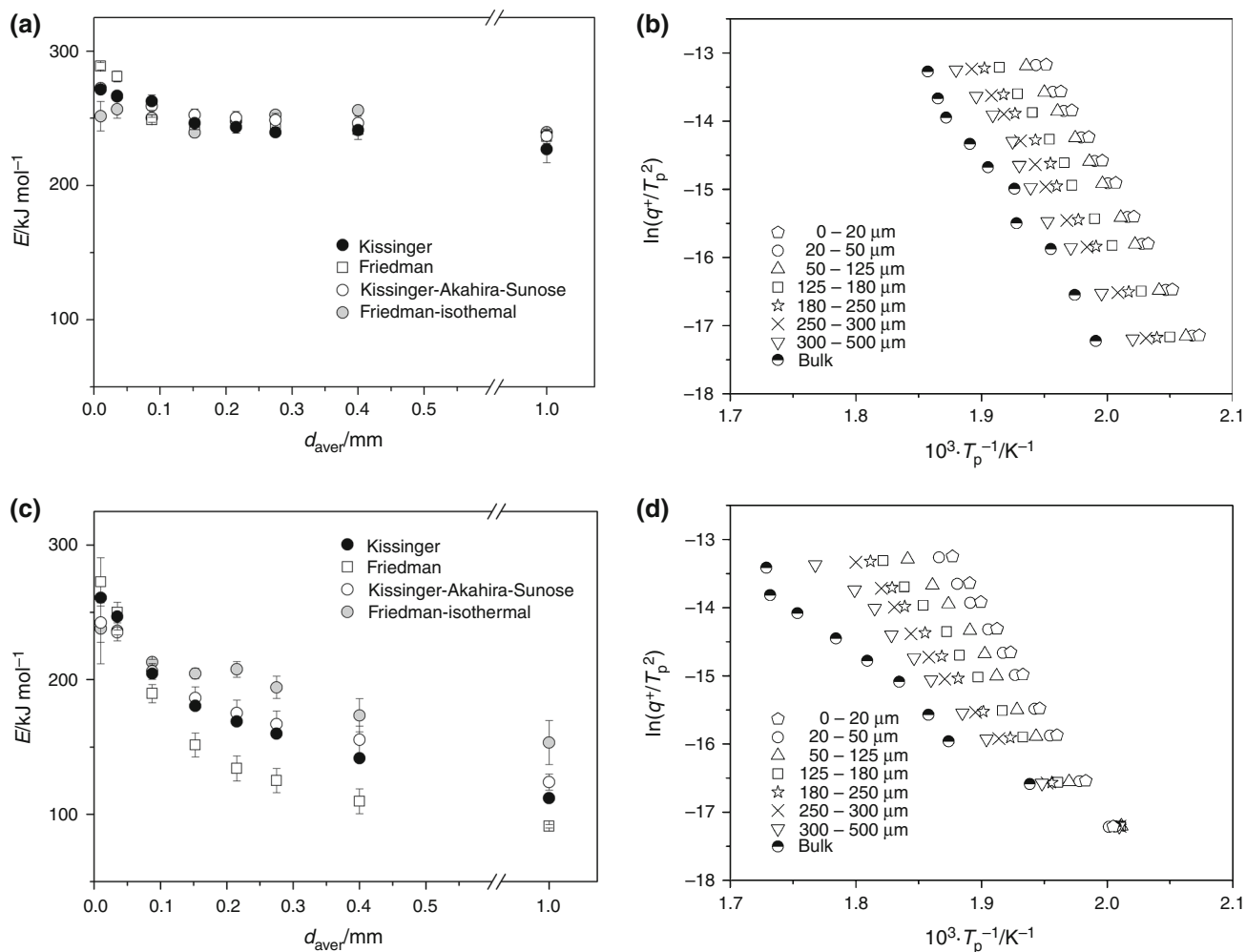


Fig. 2 **a** Comparison of apparent activation energies determined for the GeTe₄ glass according to Kissinger, Friedman (calculated for isothermal and non-isothermal data) and KAS methods dependent on average particle size. Bulk samples are assigned $d_{\text{aver}} = 1$ mm. **b** Kissinger plot constructed for all studied GeTe₄ particle size fractions. **c** Comparison of apparent activation energies determined

for the GeTe_{3.9}Se_{0.1} glass according to Kissinger, Friedman (calculated for isothermal and non-isothermal data) and KAS methods dependent on the average particle size. Bulk samples are assigned $d_{\text{aver}} = 1$ mm. **d** Kissinger plot constructed for all of the studied GeTe_{3.9}Se_{0.1} particle size fractions

crystallisation process, which will be referred to in “Identification of the crystallisation processes” section.

Further results of the kinetic analysis of the overall crystallisation processes are shown in Fig. 3; the upper and lower rows again correspond to the data from GeTe₄ and GeTe_{3.9}Se_{0.1} compositions, respectively. The graphs in Fig. 3a, c indicate that the non-isothermal crystallisation enthalpy is quite similar for both compositions and its value does not change with q^+ or d_{aver} . Similarly, also in the case of the GeTe₄ isothermal measurements (Fig. 3b), the crystallisation enthalpies did not change significantly with d_{aver} or T and corresponded to the average value obtained for non-isothermal measurements. On the other hand, the isothermal data for the GeTe_{3.9}Se_{0.1} composition (Fig. 3d) show significantly higher values of ΔH (by approximately 7 J g^{-1} ; in addition, a marked increase in

ΔH occurs for the finest powder fractions. This corresponds well to the presence of multiple crystallisation mechanisms with significantly different activation energies, where the isothermal conditions markedly emphasise domination of the one catalysed by the presence of mechanically induced defects (this is also the process with higher E). This finding is in a very good correspondence with the previously discussed results derived from the data depicted in Fig. 2.

In Fig. 4, the maxima of the non-isothermal characteristic kinetic functions $z(\alpha)$ and $y(\alpha)$ are plotted dependent on d_{aver} (note that for isothermal data, similar analysis does not provide meaningful results due to the increased separation of the involved sub-processes). In the case of simple processes, these maxima can be employed to determine the suitable kinetic model function $f(\alpha)$. However, even in the case of complex processes, these data can be utilised in

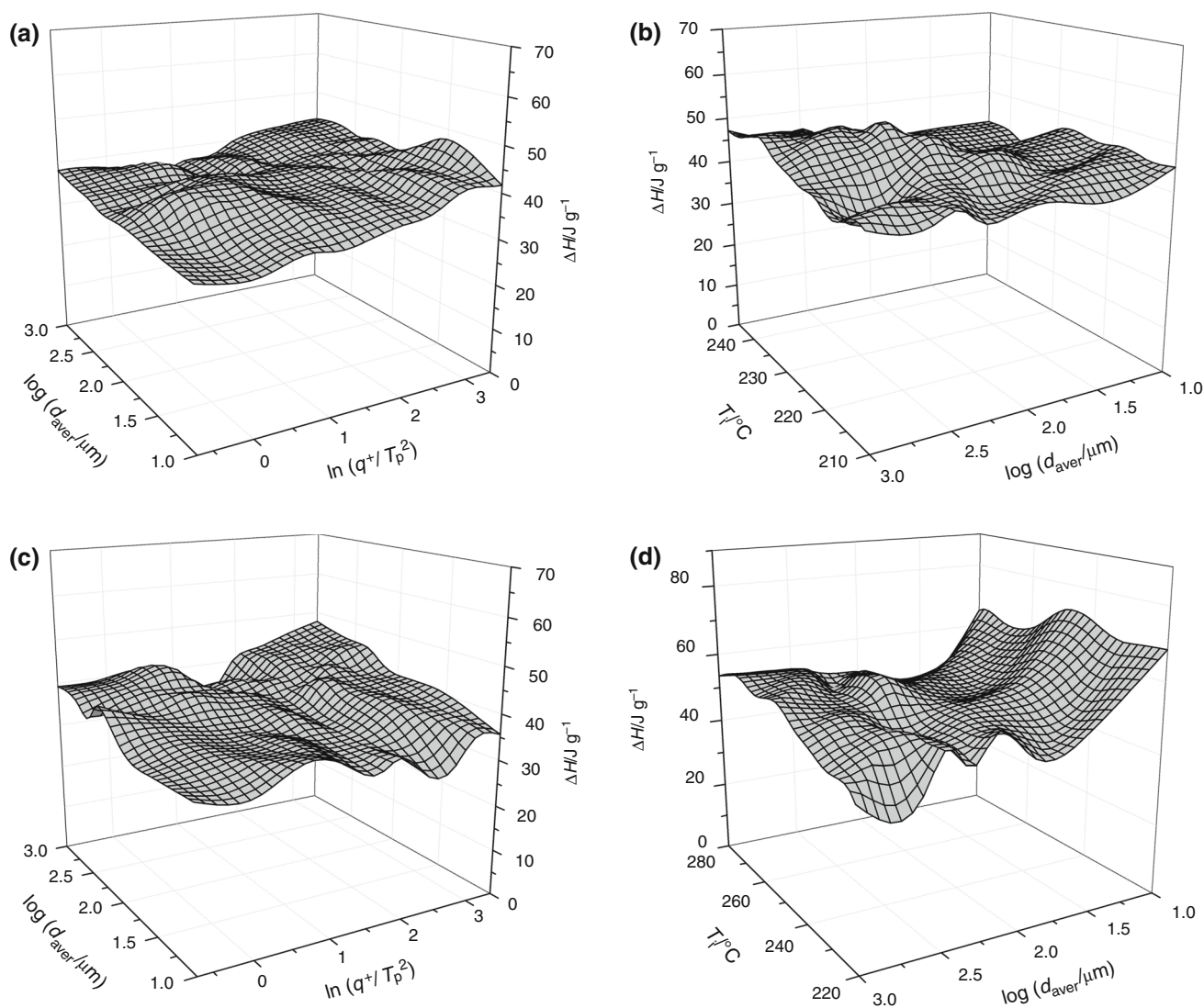


Fig. 3 Overall crystallisation enthalpy ΔH evaluated dependent on the heating rate and average particle size; **a, b** correspond to the non-isothermal and isothermal data, respectively, determined for the

GeTe_4 material; **c, d** correspond to the non-isothermal and isothermal data, respectively, determined for the $\text{GeTe}_{3.9}\text{Se}_{0.1}$ material

certain cases to estimate the dominant kinetic mechanism. The present data indicate that the substitution of Te by Se in the GeTe_4 matrix leads to an increased dominance of the JMA-like kinetic mechanisms. This is especially apparent for the fine powders (particle size fractions from 20–50 to 125–180 μm) and bulk samples. Nevertheless, without direct examination and shape analysis of the crystallisation peaks, one cannot derive more concrete conclusions regarding the nature of the involved sub-processes.

Shape analysis of the crystallisation peaks

In the present section, the strength of the direct analysis of the shape of the crystallisation peaks will be demonstrated. In order to examine the differences between the

manifestations of the particular crystallisation sub-mechanisms in the case of the two compositions studied, series of graphs depicting the respective crystallisation peaks are shown in Figs. 5 and 6. The left and right columns correspond to the GeTe_4 and $\text{GeTe}_{3.9}\text{Se}_{0.1}$ compositions, respectively. Each row then corresponds to one studied particle size, as suggested. The graphs show sets of crystallisation peaks corresponding to heating rates from 0.5 to 7 $^\circ\text{C min}^{-1}$; lower heating rates were chosen due to the better resolution of the particular overlapping mechanisms (data for the high heating rates can be found in the Supplementary online material). In the following paragraphs, the data for the respective particle size fractions of the two studied compositions will be compared. To simplify the task, the commented data will be divided according to

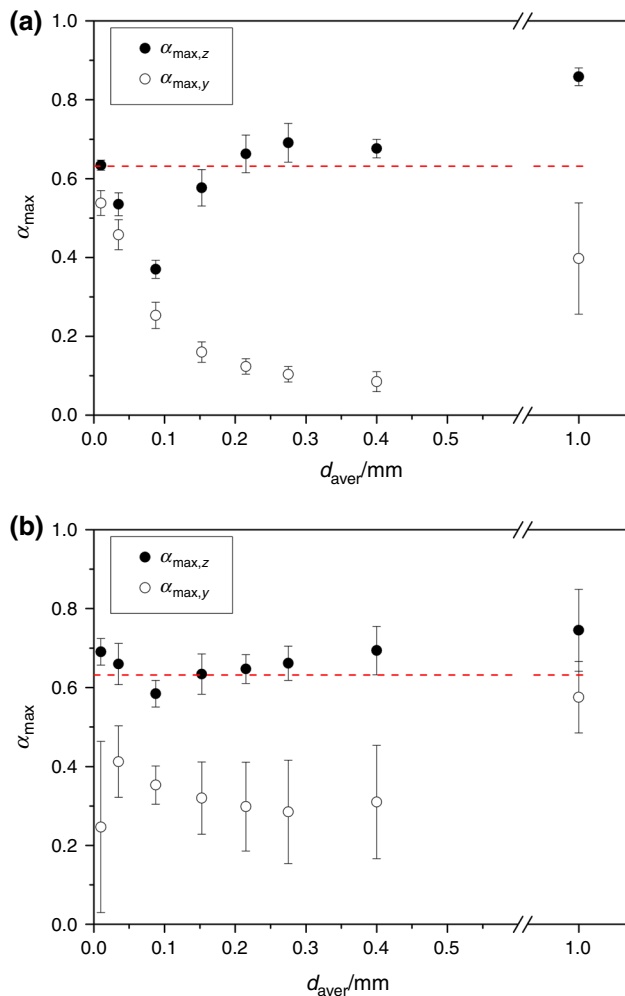


Fig. 4 Particle size dependence of the characteristic kinetic functions maxima $\alpha_{\max,z}$ and $\alpha_{\max,y}$ evaluated for the GeTe₄ data (a) and GeTe_{3.9}Se_{0.1} data (b)

particle size into four regions, in which akin kinetic behaviour occurs.

Starting with the finest powder (0–20 μm), it is apparent from Fig. 5 that the GeTe₄ composition exhibits a single peak behaviour. This crystallisation process was attributed [11, 12] to crystallisation from mechanically induced heterogeneities, where the heavily defective structure completely permeates whole glass grains. The addition of selenium clearly causes (apart from the partial repression of the dominant crystallisation process by shifting it to higher temperatures) the occurrence of a secondary crystallisation process. Looking at the deconvoluted data obtained for the heating rates of 1 and 30 $^{\circ}\text{C min}^{-1}$ (Fig. 7; data obtained for GeTe₄ at similar conditions are shown for comparison), one can see that at low heating rates (low temperatures, rather equilibrium conditions), the “secondary” process manifesting due to the presence of Se increases in magnitude. Since the dominant process (the

sharper, narrow peak) was attributed to the crystal growth from volume-located heterogeneities, we assume that the preceding secondary peak corresponds to the surface crystallisation from heterogeneities. This is confirmed by a significantly greater width of the peak, which indicates large variety of the “quality” of the crystallisation centres, features which are characteristic for the surface growth process.

Continuing with the data for the 20- to 50- and 50- to 125- μm particle size fractions, in the case of GeTe₄, the peaks gain positive asymmetry characteristic of autocatalytic processes associated with growth from mechanically induced heterogeneities surrounded by an undamaged glassy matrix. In such cases, the rather rapid growth initially catalysed by the presence of heterogeneity slows down as it proceeds throughout the undamaged glassy matrix, where the kinetic barriers are larger. [30–33] In the case of the GeTe_{3.9}Se_{0.1} composition, the peaks resemble the typical JMA behaviour, which is usually associated with the formation of a rather smaller number of larger crystallites (mechanical heterogeneities can still co-catalyse nucleation or the initial growth stages). It is also apparent that the “secondary” surface crystallisation process vanishes with increasing particle size, which is probably a consequence of the insufficiently high concentration of mechanical defects on the surface.

In the case of coarse powder fractions (from 125–180 to 300–500 μm), there is a clear occurrence of two overlapping processes in case of the GeTe₄ composition. These two processes were attributed to volume and surface growth from the mechanically induced heterogeneities [11, 12]. In the case of the GeTe_{3.9}Se_{0.1} composition, all of the considered powder fractions show a remarkably similar kinetic behaviour indicating only a very small dependence of the crystallisation mechanism on particle size. Rather low level of the process complexity suggests the dominance of one crystallisation mechanism; the reasoning in the previous paragraph then suggests that it is the volume-located growth of large crystallites which dominates at low heating rates. Increase in q^+ then leads to a more pronounced manifestation of the process complexity, possibly due to the surplus of energy and available amorphous matrix unused by the dominant JMA-like growth process.

Lastly, considering the bulk data, the crystallisation of GeTe₄ bulk glass can be described by the zero-order kinetics (F0 model). Such behaviour indicates the true surface crystallisation, where both nucleation and growth are catalysed by the surface interface and defects present at this interface. In such cases, the material is consumed at a rate of the progressing advancement of the amorphous/crystalline interface [11, 12]. In the case of the GeTe_{3.9}Se_{0.1} composition, the crystallisation data for lowest heating rates are similar to those obtained at these rates for coarse

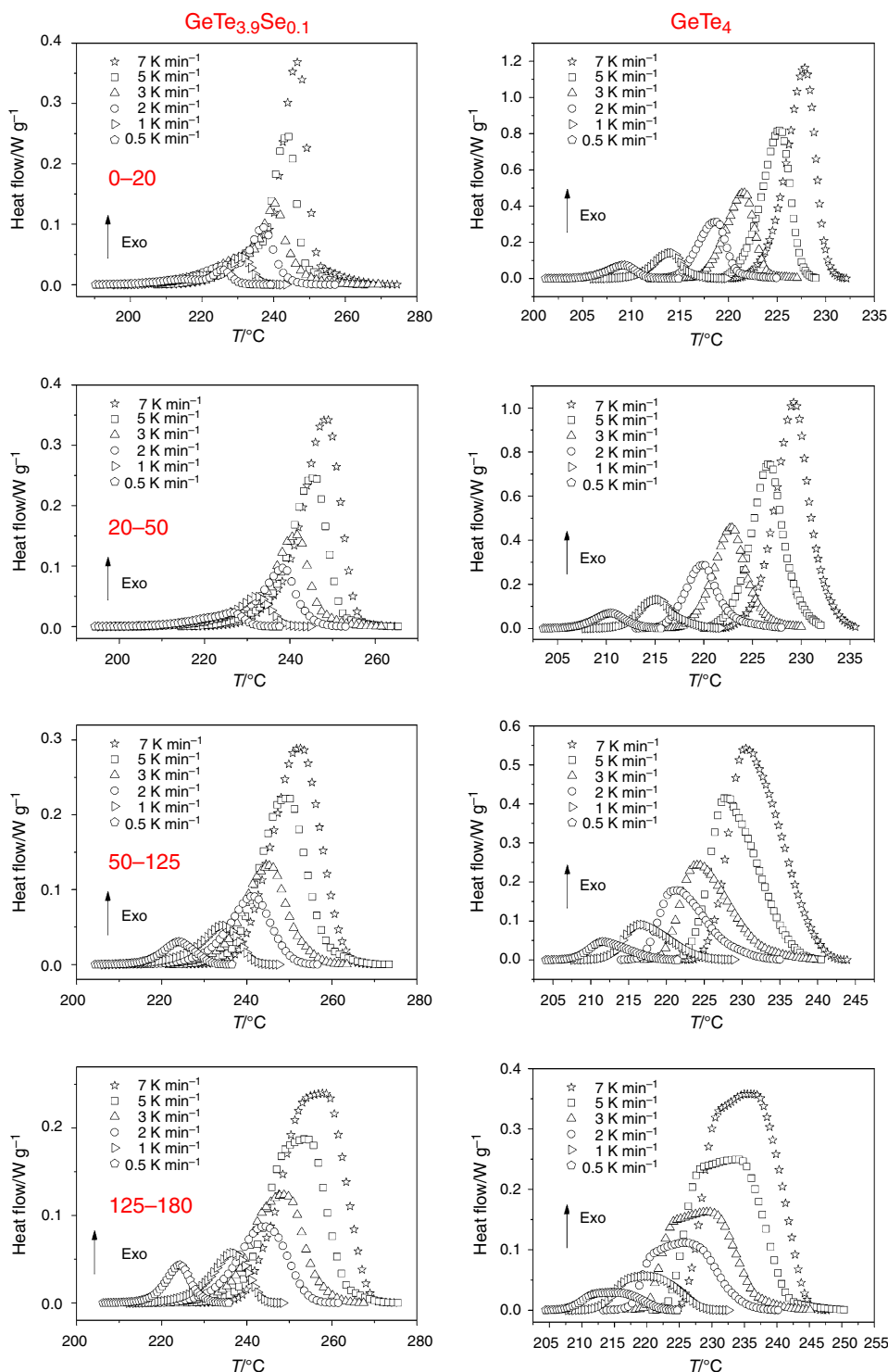


Fig. 5 Crystallisation peaks corresponding to the non-isothermal measurements of the fine particle size ranges of the two studied compositions. Particular rows match the indicated particle size

powders. This corresponds to the equality of the involved crystallisation mechanism. With increasing q^+ , the bulk samples start to exhibit crystallisation peaks with high negative asymmetry, similar to those in the case of GeTe_4

fractions; left and right columns then correspond to the data for GeTe_4 and $\text{GeTe}_{3.9}\text{Se}_{0.1}$, respectively

material. Nevertheless, the $\text{GeTe}_{3.9}\text{Se}_{0.1}$ bulk crystallisation peaks are not so sharply terminated, which indicates a possible second involved mechanism. Here, a very good correspondence with the 300- to 500- μm data can be

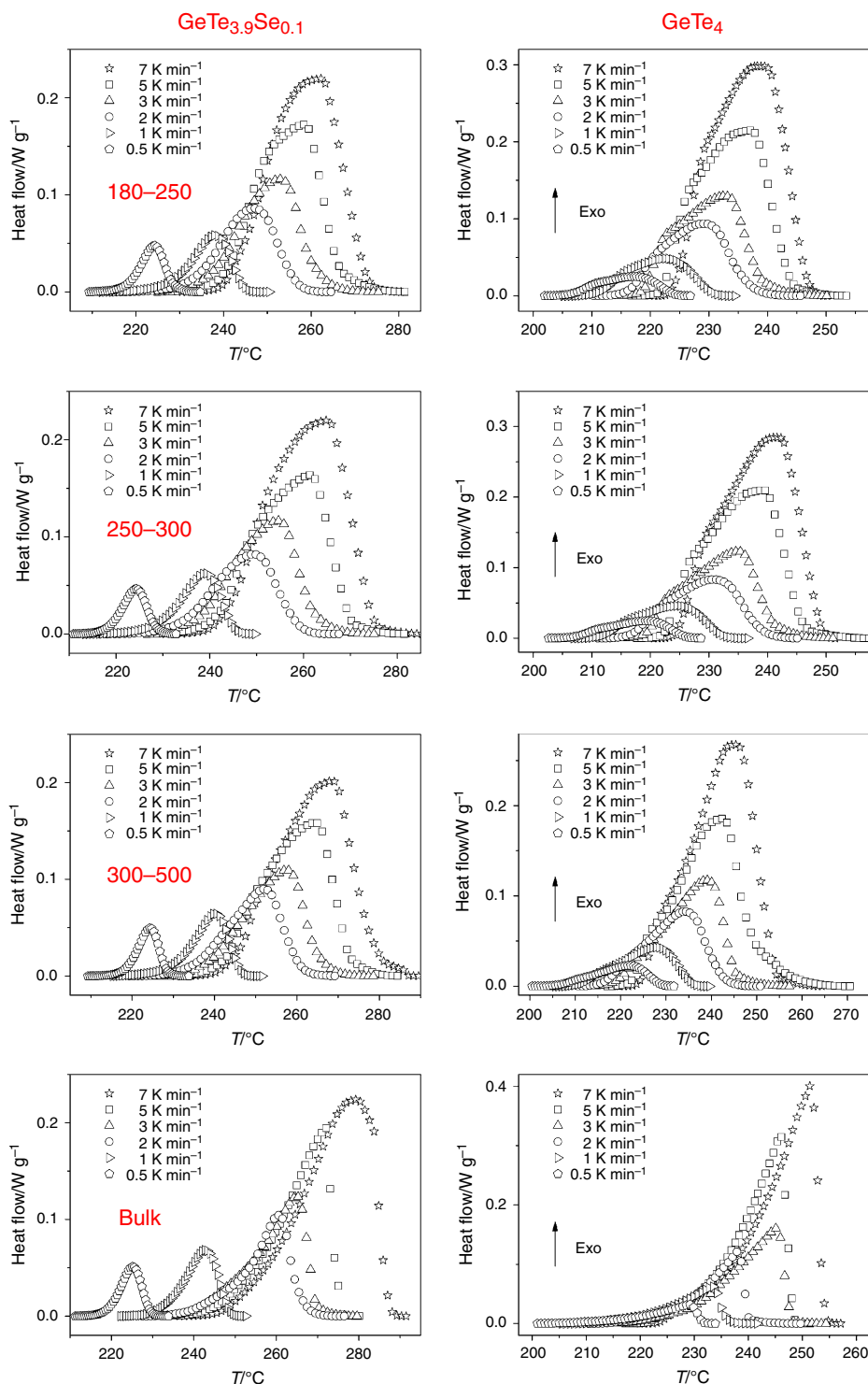


Fig. 6 Crystallisation peaks corresponding to the non-isothermal measurements of the coarse particle size ranges of the two studied compositions. Particular rows match the indicated particle size

assumed, i.e. the formation of rather large volume-located crystallites in addition to the occurring F0 surface crystal growth. The GeTe_{3.9}Se_{0.1} bulk data confirm the hypothesis introduced in the previous paragraph: Under conditions

fractions; left and right columns then correspond to the data for GeTe₄ and GeTe_{3.9}Se_{0.1}, respectively

close to equilibrium (low heating rates), the effect of Se addition is most pronounced, leading to the occurrence of JMA-like crystallisation. At higher heating rates (associated with a surplus of energy and available amorphous matrix),

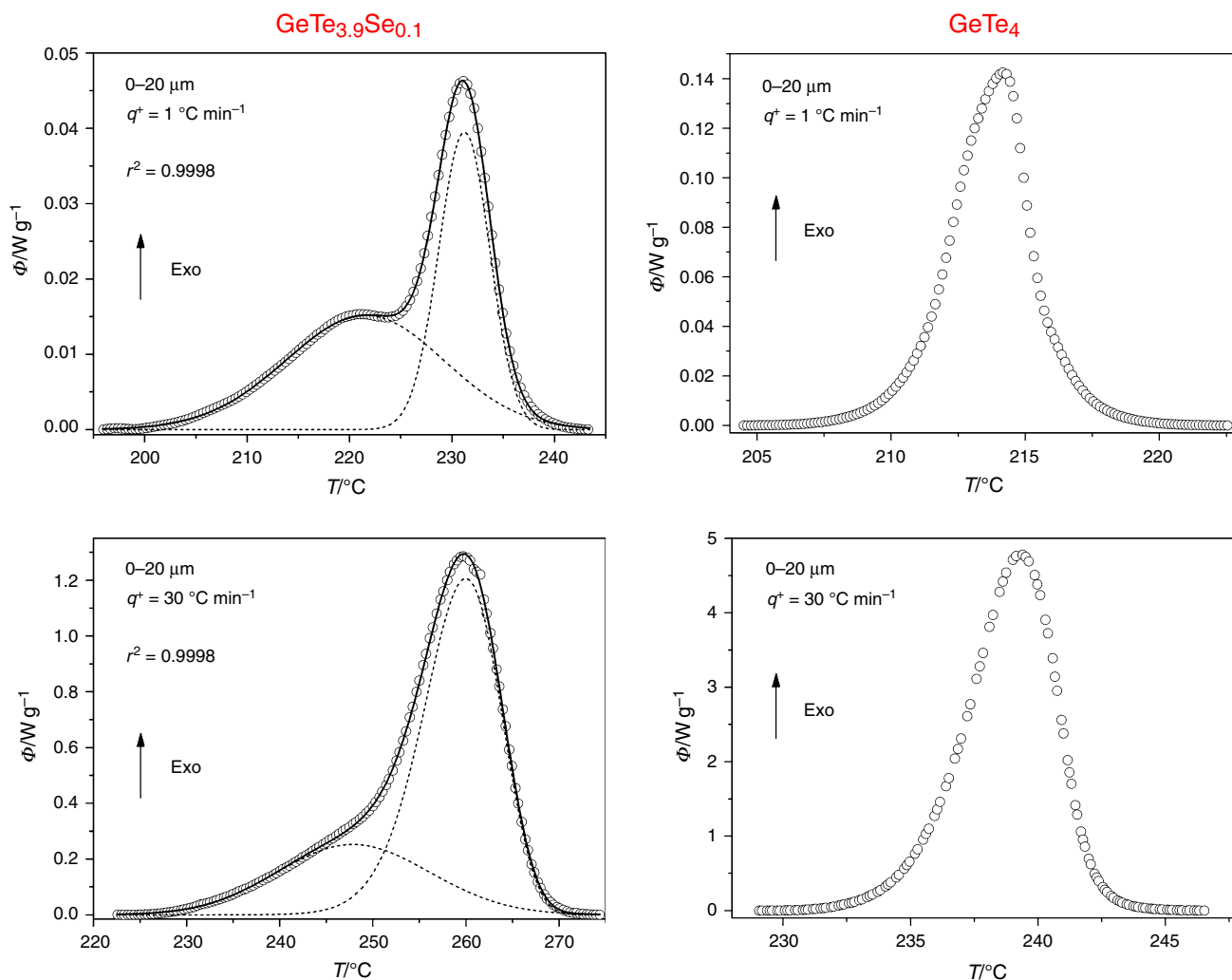


Fig. 7 Left column Fraser–Suzuki deconvolution procedure performed for the non-isothermal $\text{GeTe}_{3.9}\text{Se}_{0.1}$ crystallisation data (0- to 20- μm particle size, 1 and 30 $^{\circ}\text{C min}^{-1}$ heating rates). Dashed

lines correspond to the deconvoluted crystallisation peaks; solid line represents the overall fit of the experimental data (circles). Right column DSC data obtained for the GeTe_4 glass at similar conditions

the crystallisation behaviour of $\text{GeTe}_{3.9}\text{Se}_{0.1}$ starts to resemble that of the GeTe_4 matrix (characterised by the truly surface crystal growth); however, overlap with the JMA-like crystallisation process still occurs.

Regarding the isothermal crystallisation data, in Fig. 8, data for three typical particle size fractions are compared for the two studied chalcogenide compositions; only data corresponding to several selected annealing temperatures, T_i , are displayed in each graph for better clarity. Similar conclusions to those in the case of the non-isothermal data can also be derived for the isothermal measurements. First, it is apparent that at high temperatures, T_i (which are, again, associated with surplus of energy and available amorphous material), the crystallisation behaviour is very similar for both compositions. This is in good agreement with that which was expected; i.e. in the case of isothermal measurements, the dominant crystallisation mechanism

increases in its magnitude due to the following factors: enhanced effect of differences of apparent activation energies (contrary to non-isothermal measurements, wide temperature range is not explored), and significantly shortened time for nucleation ($q^+ = 100 \text{ }^{\circ}\text{C min}^{-1}$ was applied to get to T_i). The differences between the crystallisation kinetics of the two studied compositions arise at low T_i temperatures (insets in the respective graphs in Fig. 8). In the case of fine powders (here represented by the 0- to 20- μm particle size fraction), the Se \leftrightarrow Te substitution leads to the enhanced manifestation of the first-order kinetic mechanism (sharply decreasing peaks with maximum at $\alpha = 0$), which is often associated with the surface crystallisation from mechanically induced heterogeneities [34, 35]. In the case of bulk samples annealed at low T_i s, on the other hand, the Se \leftrightarrow Te substitution results in a large slowly evolving peak occurring at high α and overlapping

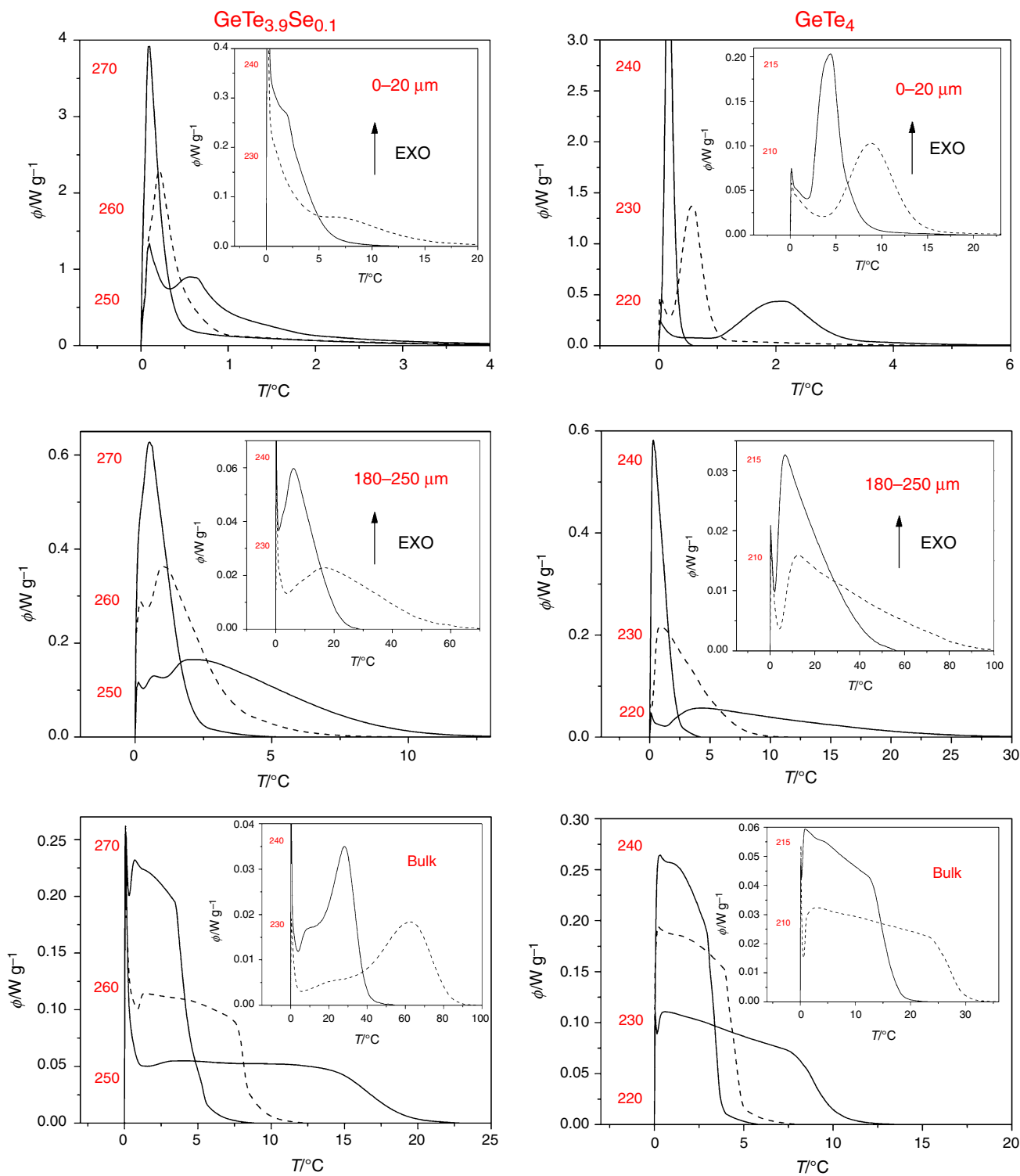


Fig. 8 Isothermal crystallisation data for the three chosen particle size fractions of the two studied compositions. Particular rows match the indicated particle size fractions; *left and right columns* then correspond to the data for GeTe₄ and GeTe_{3.9}Se_{0.1}, respectively. The

respective T_i values are displayed next to the maxima of the corresponding isothermal DSC peaks; *insets* the data for low annealing temperatures

with the underlying zero-order kinetic mechanism. The shape and position of this peak correspond well to a three-dimensional growth of volume-located crystallites. [34, 35]

As can be seen, the above-listed conclusions are in perfect correspondence with the results obtained for the non-isothermal data.

Identification of the crystallisation processes

In the last section of the present article, the particular crystallisation mechanisms and processes described in the previous paragraphs will be identified and confirmed by means of infrared microscopy and XRD.

The crystallisation processes occurring in the GeTe_4 material are documented by the infrared micrographs displayed in Fig. 9. The micrographs A and B show the evolution of the sample surface crystalline microstructure with increasing degree of conversion α (views from above). Picture A represents a very early stage of the crystallisation process, where the initial very thin layer of fine microcrystals is formed. This layer grows in time and becomes rougher (micrograph B) as the growing laminae start to overlap. Partially crystallised bulk sample in cross section is displayed in Fig. 9c. The thickness of the surface layer is highly uniform and increases linearly with time as it grows inwards until the sample is fully crystalline. This indicates a true crystallisation from surface defects, characteristic for the manifestation of the zero-order kinetics (F0), which was indeed determined for the GeTe_4 bulk samples. Note that in the case of bulk sample crystallisation, there were no volume-located nuclei/crystallites and the growth proceeded strictly from surface defects. A completely different situation arose in case of powder samples. Micrograph D

shows piece of a crushed glass grain from the 125- to 180- μm particle size fraction, which underwent partial crystallisation (only a very early stage of crystallinity equal to approximately 1 % of the overall ΔH was reached). The right and bottom borders of the grain piece glare, which indicates the formation of a thin surface layer of crystallites (the crushed grain is displayed in cross section in this regard). In addition, at closer inspection, several bright dots can be recognised in the volume of the glass grain, which correspond to the initial tiny crystals being formed. Compared to the crystallisation behaviour of the bulk (undamaged) GeTe_4 material, the volume-located crystallites occurring in case of the GeTe_4 powders clearly need to be originating from the mechanically induced heterogeneities. This again corresponds well to the results of the kinetic analysis presented in “[Shape analysis of the crystallisation peaks](#)” section.

The crystallisation of the $\text{GeTe}_{3.9}\text{Se}_{0.1}$ glass studied by infrared microscopy is presented in Fig. 10. The micrographs A and B again show the evolution of the surface crystalline layer (views from above) with increasing α . The initial stage of crystallisation is shown in Fig. 10a; in addition to the fine crystalline microstructure covering the surface (similarly as in case of GeTe_4), occasional “islands” of separated microcrystals are formed. Micrograph 10b then represents the surface of a fully crystalline

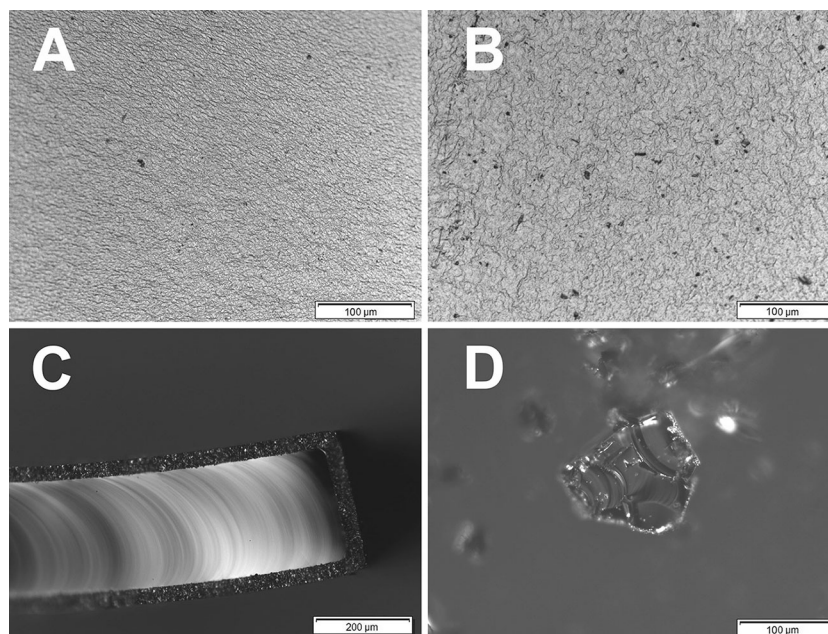


Fig. 9 Micrographs obtained by means of infrared microscopy for the GeTe_4 samples. **a** Surface layer of fine crystallites formed in the early stage of the initial crystallisation process (view from above). The scaling abscissa indicates a length of 50 μm . **b** Surface crystalline layer formed at the late stage of the crystallisation process (view from above). The scaling abscissa indicates a length of 50 μm . **c** Cross-

section view of a partially crystallised plate-like bulk sample-crystalline surface layer encloses the (yet) amorphous core. The scaling abscissa indicates a length of 200 μm . **d** Crushed partially crystallised grain of the GeTe_4 125- to 180- μm powder. The scaling abscissa indicates a length of 50 μm

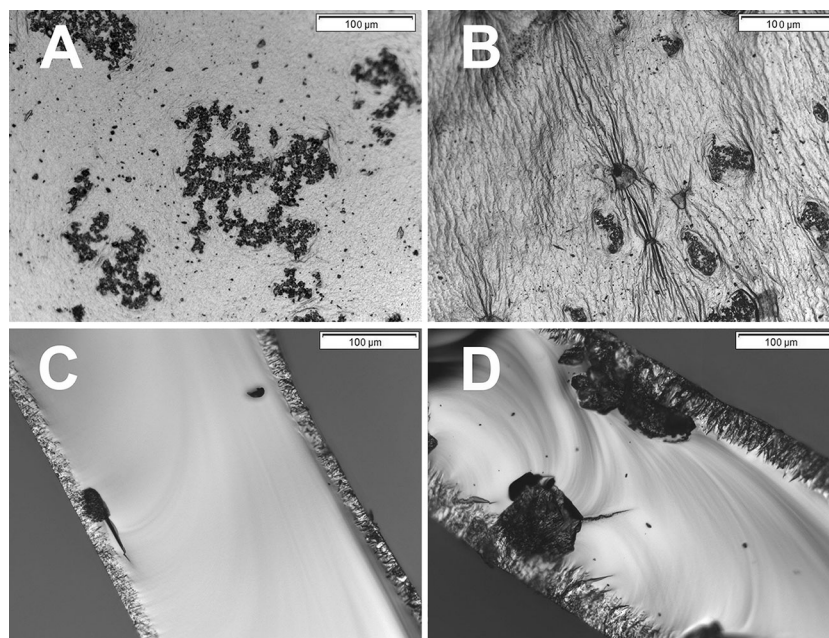


Fig. 10 Micrographs obtained by means of infrared microscopy for the GeTe_{3.9}Se_{0.1} samples. **a** Surface crystalline layer formed in the early stage of the initial crystallisation process (*view from above*). The *scaling abscissa* indicates a length of 50 μm. **b** Surface crystalline layer formed at the late stage of the crystallisation process (*view from above*). The *scaling abscissa* indicates a length of 100 μm. **c** Cross-section view of a partially crystallised plate-like bulk sample (early

stage of crystallisation). Thin crystalline surface layer encloses the (yet) amorphous core; first bulk crystallites are being formed. The *scaling abscissa* indicates a length of 50 μm. **d** Cross-section view of a partially crystallised plate-like bulk sample (advanced stage of the crystallisation process). Surface crystalline layer is thicker; bulk crystallites are larger. The *scaling abscissa* indicates a length of 50 μm

GeTe_{3.9}Se_{0.1} glass. As can be seen, the initially formed “islands” of small crystallites remained isolated as the original fine underlying crystalline layer increased in thickness and produced a highly corrugated surface. Moreover, certain characteristic defects appearing as corrugation origins/centres can be found at the sample surface. These usually correspond to the ridges of large crystals formed under the surface and extruding the compact surface layer out.

Micrographs 10c, d then show the cross section of partially crystallised GeTe_{3.9}Se_{0.1} bulk samples. If we compare these micrographs to that of the GeTe₄ sample (Fig. 9c), several differences are evident. The first consequence of the Se ↔ Te substitution is that the GeTe_{3.9}Se_{0.1} surface layer has a significantly different structure on the cross section. Instead of the highly consistent sheet composed of tiny microcrystals (found for GeTe₄), the GeTe_{3.9}Se_{0.1} surface layer appears to be a conglomerate of larger crystallites originating at surface and growing inwards, forming a typical spiky crystalline/amorphous interface. The second, more important effect of the Se ↔ Te substitution is the formation of large volume-located crystals. Looking at Fig. 10c, the growth of these crystals can originate either from true CNT nuclei or from nuclei/defects that are formed at the above-mentioned spiky crystalline/amorphous interface produced

by the growing surface layer. Figure 10d then shows that it is the latter type of crystallisation that is preferred; while the growth of the crystallites attached to the surface layer proceeds rapidly, the volume-located nuclei seem to grow only very slowly. During further heating (or annealing), the formation of large volume-located crystals absolutely dominates. The surface layer stops to grow (most probably due to the absence of the available amorphous matrix at the inner interface) and the large crystals, similar to those depicted in Fig. 10d, fill the internal volume. These findings again correspond well to the results provided by the shape analysis of the DSC crystallisation peaks presented in “[Shape analysis of the crystallisation peaks](#)” section.

Lastly, we used infrared microscopy to study the partially crystallised GeTe_{3.9}Se_{0.1} powder. Again, for the initial crystallisation stages, we have found a significant number of volume-located microcrystals consistent with the growth from mechanically induced heterogeneities (micrographs similar to that shown in Fig. 9d were obtained). However, the quality of the micrographs was not sufficient to reliably distinguish between the GeTe₄ and GeTe_{3.9}Se_{0.1} compositions. In the case of higher crystallinity degrees, even the largest powder grains (similarly as for GeTe₄) broke into many very small pieces, indicating a large number of volume-located crystallites.

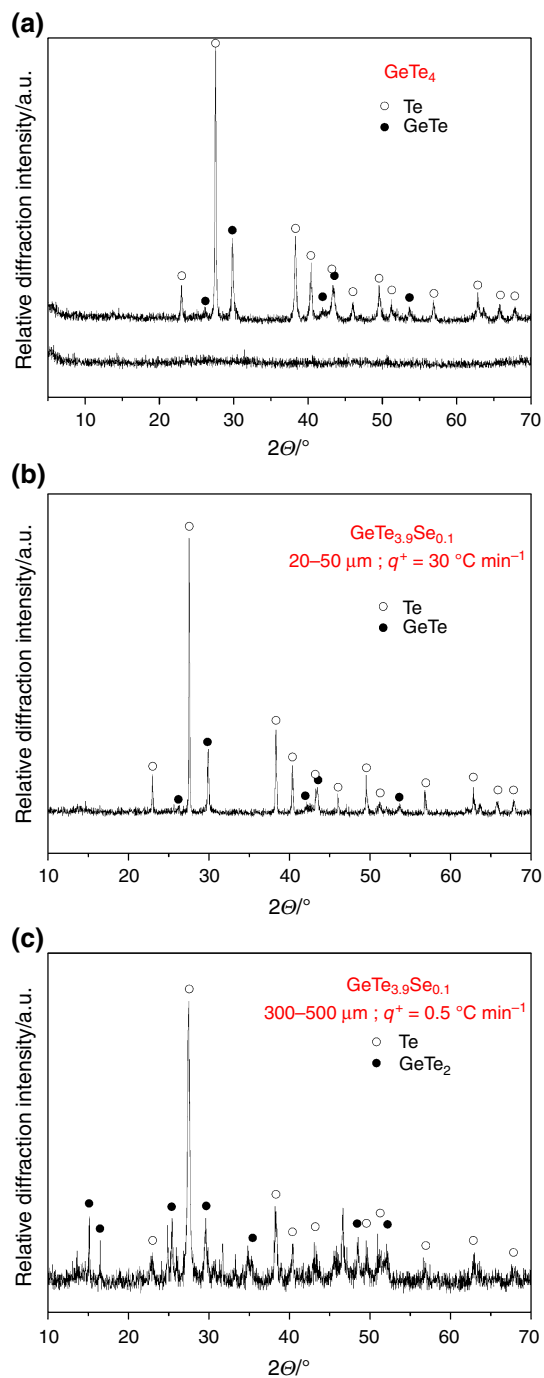


Fig. 11 **a** Diffraction patterns of amorphous (*lower pattern*) and crystallised (*upper pattern*) GeTe_4 . The particular diffraction lines corresponding to Te and GeTe are indicated. **b** Diffraction pattern of crystallised $\text{GeTe}_{3.9}\text{Se}_{0.1}$ glass. The particular diffraction lines corresponding to Te and GeTe are indicated. **c** Diffraction pattern of slowly crystallised coarse $\text{GeTe}_{3.9}\text{Se}_{0.1}$ powder. The particular diffraction lines corresponding to Te and GeSe_2 are indicated

In order to identify the crystalline phases, an XRD analysis of both compositions was performed which was dependent on the experimental conditions applied during

the crystallisation. In the case of the GeTe_4 glass, all of the diffractograms provided similar results; a representative case is shown in Fig. 11a together with the data for an amorphous as-prepared sample (lower line). Regarding the identification of the crystalline phases, hexagonal tellurium (P3121, $a = 4.4572$, $b = 4.4572$, $c = 5.9290$) is the main crystalline phase, accompanied by rhombohedral GeTe (R3 m, $a = 8.3280$, $b = 8.3280$, $c = 10.690$). Very similar results were also found for the diffractograms of $\text{GeTe}_{3.9}\text{Se}_{0.1}$ fine powders (all heating rates) and coarse powders (only high heating rates); for a representative example of these diffractograms, see Fig. 11b. Note that most intense XRD signals corresponding to the presence of well-formed crystals were obtained at high heating rates. A different situation arises for coarse powders crystallised at low heating rates (see Fig. 11c), i.e. at equilibrium-like conditions. The grains are only poorly crystalline and, apart from the dominant hexagonal tellurium, the samples contain also monoclinic GeSe_2 (P21/c, $a = 7.016$, $b = 16.796$, $c = 11.831$, $\alpha = 90^\circ$, $\beta = 90.65^\circ$, $\gamma = 90^\circ$) and at least one more unidentified crystalline phase (possibly combined Ge–Te–Se crystallites). These findings correspond very well to those provided by infrared microscopy, indicating that at experimental conditions associated with small driving force (low q^+ , low T_i) and a low number of mechanically induced heterogeneities, significantly different crystallisation processes manifest and different crystalline phases are formed.

Conclusions

The addition of selenium was found to markedly influence the crystallisation kinetics, prioritising the slower nucleation–growth type of crystallisation over the fast autocatalytic growth from defects. This effect is more enhanced when the crystallisation conditions with greater equilibrium are applied (slow heating rates q^+ or low annealing temperatures T_i).

Regarding the crystal morphology, the addition of selenium leads to the occurrence of a smaller number of larger crystallites, which confirms the suppressing effect of Se influencing the nucleation process. The surface layer of fine crystallites is found only in the very early stages of crystallisation for the $\text{GeTe}_{3.9}\text{Se}_{0.1}$ material and is soon outgrown by a layer of larger crystals enlarging dominantly in the inwards direction. The main effect of the addition of Se lies in the occurrence of large volume-located crystallites exhibiting a genuine three-dimensional growth.

The XRD analysis confirmed that in cases when large number mechanical defects are present or an energy surplus is provided, similar crystalline phases (Te and GeTe) form as for the pure GeTe_4 . On the other hand, the practical

absence of mechanically induced heterogeneities together with a low crystallisation driving force leads to the formation of significantly different crystalline phases containing selenium. We have shown previously [28, 29, 36] that selenium (compared to Te-rich Se–Te chalcogenide matrices) leads to nucleation–growth-based formation of large slowly growing crystallites. The present findings show that a similar effect is responsible for the markedly enhanced glass stability and glass-forming ability of Se-doped GeTe₄ infrared glass.

Acknowledgements This work has been supported by the Czech Science Foundation under Project No. P106/11/1152.

References

- Cui S, Chahal R, Boussard-Plédel C, Nazabal V, Doualan JL, Troles J, Lucas J, Bureau B. From selenium- to tellurium-based glass optical fibers for infrared spectroscopies. *Molecules*. 2013;18:5373–88.
- Maurugeon S, Boussard-Plédel C, Troles J, Faber AJ, Lucas P, Zhang XH, Lucas J, Bureau B. Telluride glass step index fiber for the far infrared. *J Lightwave Technol*. 2010;28:3358–63.
- Wang G, Nie Q, Wang X, Dai S, Xu T, Shen X, Zhang X. Composition dependence of optical band gap of the Se–Ge–Te far infrared transmitting glasses. *Phys B*. 2010;405:4424–8.
- Conseil C, Shiryayev VS, Cui S, Boussard-Plédel C, Troles J, Velmuhov AP, Potapov AM, Suchkov AI, Churbanov MF, Bureau B. Preparation of high purity Te-Rich Ge–Te–Se fibers for 5–15 μm infrared range. *J Lightwave Technol*. 2013;31:1703–7.
- Zhang SN, He J, Zhu TJ, Zhao XB, Tritt TM. Thermal conductivity and specific heat of bulk amorphous chalcogenides Ge₂₀Te_{80-x}Se_x (x = 0,1,2,8). *J Non-Cryst Sol*. 2009;355:79–83.
- Sharma P, Katyal SC. Far-infrared transmission and bonding arrangement in Ge₁₀Se_{90-x}Te_x semiconducting glassy alloys. *J Non-Cryst Sol*. 2008;354:3836–9.
- Zavadil J, Kostka P, Pedlikova P, Zdansky K, Kubliha M, Labas V, Kaluzny J. Electro-optical characterization of Ge–Se–Te glasses. *J Non-Cryst Sol*. 2009;355:2083–7.
- Sarrach DJ, deNeufville JP, Haworth HL. Studies of amorphous Ge–Se–Te alloys (II): thermal crystallization of sputtered Ge₂₀Se₄₀Te₄₀. *J Non-Cryst Sol*. 1978;27:193–208.
- Maurugeon S, Bureau B, Boussard-Plédel C, Faber AJ, Lucas P, Zhang XH, Lucas J. Selenium modified GeTe₄ based glasses optical fibers for far-infrared sensing. *Opt Mater*. 2011;33:660–3.
- Maurugeon S, Bureau B, Boussard-Plédel C, Faber AJ, Zhang XH, Geliessen W, Lucas J. Te-rich Ge–Te–Se glass for the CO₂ infrared detection at 15 μm. *J Non-Cryst Sol*. 2009;355:2074–8.
- Svoboda R, Brandová D, Málek J. Non-isothermal crystallization kinetics of GeTe₄ infrared glass. *J Therm Anal Calorim*. 2015. doi:10.1007/s10973-015-4937-x.
- Svoboda R, Brandová D. Crystallization from mechanically induced defects—a phenomenon observed for chalcogenide glasses. *J Therm Anal Calorim*. (submitted).
- Šesták J. Thermophysical properties of solids, their measurements and theoretical analysis. Amsterdam: Elsevier; 1984.
- Kissinger HE. Reaction kinetics in differential thermal analysis. *Anal Chem*. 1957;29:1702–6.
- Friedman HL. Kinetics of thermal degradation of char-forming plastics from thermogravimetry. Application to a phenolic plastic. New York: Wiley; 1964.
- Starink MJ. The determination of activation energy from linear heating rate experiments: a comparison of the accuracy of iso-conversion methods. *Thermochim Acta*. 2003;404:163–76.
- Málek J. Kinetic analysis of crystallization processes in amorphous materials. *Thermochim Acta*. 2000;355:239–53.
- Málek J. The kinetic analysis of non-isothermal data. *Thermochim Acta*. 1992;200:257–69.
- Avrami M. Kinetics of phase change I—general theory. *J Chem Phys*. 1939;7:1103–12.
- Avrami M. Kinetics of phase change. II—transformation-time relations for random distribution of nuclei. *J Chem Phys*. 1940;7:212–24.
- Avrami M. Granulation, phase change, and microstructure—kinetics of phase change III. *J Chem Phys*. 1941;7:177–84.
- Johnson WA, Mehl KF. Reaction kinetics in processes of nucleation and growth. *Trans Am Inst Min (Metall) Eng*. 1939;135:416–42.
- Khawam A, Flanagan DR. Solid-state kinetic models: basics and mathematical fundamentals. *J Phys Chem B*. 2006;110:17315–28.
- Vyazovkin S, Burnham AK, Criado JM, Pérez-Maqueda LA, Popescu C, Sbirrazzuoli N. ICATC Kinetics Committee recommendations for performing kinetic computations on thermal analysis data. *Thermochim Acta*. 2011;520:1–19.
- Hrubý A. Evaluation of glass-forming tendency by means of DTA. *Czechoslov. J Phys B*. 1972;22:1187–93.
- Weinberg MC. An assessment of glass stability criteria. *Phys Chem Glasses*. 1994;35:119–23.
- Lu ZP, Liu CT. A new glass-forming ability criterion for bulk metallic glasses. *Acta Mater*. 2002;50:3501–12.
- Svoboda R, Málek J. Thermal behavior in Se-Te chalcogenide system: interplay of thermodynamics and kinetics. *J Chem Phys*. 2014;141:224507-1–10.
- Svoboda R, Málek J. Thermal behavior of Se-rich Ge₂Sb₂Se_(5-y)Te_y chalcogenide system. *J Alloys Compd*. 2015;627:287–98.
- Svoboda R, Brandová D, Málek J. Crystallization behavior of GeSb₂Se₄ chalcogenide glass. *J Non-Cryst Sol*. 2014;388:46–54.
- Svoboda R, Bezdička P, Gutwirth J, Málek J. Crystallization processes in Ge₂Sb₂Se₄Te glass. *Mater Res Bull*. 2015;61:207–14.
- Svoboda R, Málek J. Crystallization mechanisms occurring in Se–Te glassy system. *J Therm Anal Calorim*. 2015;119:155–66.
- Svoboda R, Málek J. Amorphous-to-crystalline transition in Te doped Ge₂Sb₂Se₅ glass. *J Therm Anal Calorim*. 2014;117:1073–83.
- Svoboda R, Málek J. Interpretation of crystallization kinetics results provided by DSC. *Thermochim Acta*. 2011;526:237–51.
- Svoboda R, Málek J. Particle size influence on crystallization behavior of Ge₂Sb₂Se₅ glass. *J Non-Cryst Sol*. 2012;358:276–84.
- Svoboda R, Málek J. Extended study of crystallization kinetics for Se–Te glasses. *J Therm Anal Cal*. 2013;111:161–71.